Journal of Advanced Research in Ocean Engineering 1(1) (2015) 001-013
http://dx.doi.org/10.5574/JAROE.2015.1.1.001

SPH Modeling of Hydraulics and Erosion of HPTRM Levee

Lin Li[1], Xin Rao[2], Farshad Amini[1*], and Hongwu Tang[3]

[1] *Department of Civil and Environmental Engineering, Jackson State University, Jackson, Mississippi, 39217, USA*

[2] *Laboratory for Fishing Technology and Fishery Engineering, East China Sea Fishery Research Institute, Chinese Academy of Fishery Sciences, Shanghai, China*

[3] *State Key Laboratory of Hydrology-Water Resources and Hydraulic Engineering, Hohai University, Nanjing, China*

(Manuscript Received December 5 2014; Revised January 6, 2015; Accepted Fevruary 2, 2015)

Abstract

Post-Katrina investigations revealed that most earthen levee damage occurred on the levee crest and landward-side slope as a result of either wave overtopping, storm surge overflow, or a combination of both. In this paper, combined wave overtopping and storm surge overflow of a levee embankment strengthened with high performance turf reinforcement mat (HPTRM) system was studied in a purely Lagrangian and meshless approach, two-dimensional smoothed particle hydrodynamics (SPH) model. After the SPH model is calibrated with full-scale overtopping test results, the overtopping discharge, flow thickness, flow velocity, average overtopping velocity, shear stress, and soil erosion rate are calculated. New equations are developed for average overtopping discharge. The shear stresses on landward-side slope are calculated and the characteristics of soil loss are given. Equations are also provided to estimate soil loss rate. The range of the application of these equations is discussed.

Keywords: High performance turf reinforcement mat, smoothed particle hydrodynamics, levee, erosion, overtopping, shear stress

1. Introduction

Earthen levees and dikes are used throughout the world to protect populations and infrastructure from periodic floods and high water due to storm surges. Overtopping may occur during the periods of flood due to insufficient freeboard. The most problematic case involves the levee being overtopped by both surge and waves when the surge level exceeds the levee crest elevation with accompanying wave overtopping [1]. Overtopping of earthen levees produces fast-flowing, turbulent water velocities on the landside slope that can damage the protective grass covering and expose the underlying soil to erosion [2]. If overtopping continues long enough, the erosion may eventually result in loss of levee crest elevation and perhaps breaching of the protective structure. Hurricane Katrina caused the levee system that surrounds the New Orleans experienced catastrophic overtopping and extensive damage [3, 4]. Post-Katrina investigations revealed that most earthen levee damage occurred on the levee crest and landward-side slope as a result of either wave overtopping, storm surge overflow, or a combination of both [5]. Hence, the crest and landside slopes of those levees that are at risk of overtopping must be protected with some types of strengthening method such as turf reinforcement, soil strengthening, or hard armoring. The levee strengthening systems

[*] Corresponding author. Tel.: +1-601-9793913, Fax.: +1-601-9793238,
E-mail address: famini@jsums.edu

should resist the forces of fast-flowing, turbulent water that has overtopped the levee crest. High performance turf reinforcement mat is one of the strengthening systems that can be used on the crest and landward-side of earthen levee.

High performance turf reinforcement mat (HPTRM) is one of the most advanced flexible armoring technologies available today for severe erosion challenges. The HPTRMs are three-dimensional TRMs joined at the intersections of randomly oriented nylon filaments with high tenacity polyester geogrid reinforcement at low strains. Nearly 95% of space is open space in this material. As the grass roots grow through the open space of HPTRM, roots become entwined within the turf reinforced mat (Fig. 1). The interlocking between roots and HPTRM can enhance the roots resistance against hydraulic life and shear forces created by high water flow hydraulic erosion. A specific gravity of nylon in the HPTRM more than 1.0 ensures that the HPTRM will not float under any hydraulic condition. The geogrid reinforcement in the HPTRM can help soil stabilization mechanically by taking over when extreme conditions exist.

A full-scale study on combined wave and surge overtopping of a levee armored with HPTRM was conducted in Large Wave Flume in The O.H. Hinsdale Wave Research Laboratory (HWRL) at Oregon State University. Based on the measured flow thickness and flow velocity on crest and landward-side slope, new equations are developed to estimate distribution of instantaneous discharge, distribution of individual wave volumes as well as detailed flow parameters on landward-side slope, e.g. mean flow thickness, RMS wave height, mean velocity, and velocity of the wave front [6].

Levee breach problems are often numerically solved using traditional grid – based numerical methods such as the finite difference methods (FDM) and the finite element methods (FEM). Since the levee breach usually occurs under wave condition and as a result of wetting–drying flood phenomena, the smoothed particle hydrodynamics (SPH) method is more apropriate to address the moving domain problems [7, 8, 9, 10]. The SPH has been employed to study the wave overtopping over coastal structures [11, 12, 13, 14].

SPH is a gridless, pure Lagrangian method for solving the equations of fluid dynamics. In this approach, the particles are interpolation points from which properties of the fluid can be calculated. The SPH can deal with large deformations of the free surface and interface problems without requiring grid or mesh refinement for any change in density, viscosity, and flow morphology. In the SPH conception, the motion of each particle is calculated through the interactions with the neighbouring particles using an analytical kernel function. All terms in the governing equations can be represented by the particle interaction models and thus a grid is not needed. Grid is not needed because renormalizations techniques rely on background grids. These features of the SPH are very useful for a two-phase flow with water–structure interactions. During the past years, considerable efforts have been devoted to enhance the performance of SPH method [15,16]. Furthermore, several recent studies have been carried out on particle-based simulation of erosion processes [17, 18].

Fig.1. Illustrations of vegetated HPTRM system. The open space of HPTRM allows roots grow through and entwined with the HPTRM to reinforce the plant roots.

In this paper, the SPH method is used to predict the hydraulic performance of the HPTRM strengthened earthen levee during combined wave and surge turbulent overtopping conditions. After verifying the SPH model with full-scale overtopping experimental results, new equations are developed to estimate overtopping discharge. The shear stress on landward-side slope and levee crest are calculated. The characteristics of soil loss rate on HPTRM-strengthened levee are also given.

2. Numerical Methodology

2.1. Sph Method For Levee Overtopping

The Lagrangian form of the governing equations was used in the SPH model. The mass and momentum equations of the particle-scale flow can be derived from the Navier-Stokes (N-S) equations as follows:

$$\frac{1}{\rho}\frac{d\rho}{dt} + \nabla \cdot \mathbf{u} = 0 \tag{1}$$

$$\frac{d\mathbf{u}}{dt} = -\frac{1}{\rho}\nabla P + f / m + \nu_o \nabla^2 \mathbf{u} \tag{2}$$

where ρ is water density, t is time, $\boldsymbol{u}$ is water velocity, P is water pressure, f is external force, m is mass, and $_o$ is laminar kinematic viscosity. The laminar kinematic viscosity was replaced by an artificial viscosity in the following formula [7].

To find the value of a particular quantity f at an arbitrary point, x, an interpolation is applied [19]:

$$f(x) = \sum_j f_j w(x - x_j) V_j \tag{3}$$

where f_j is the value of f associated with particle j located at x_j, $w(x\text{-}x_j)$ is a weighting of the contribution of particle j to the value of $f(x)$ at position x, and V_j is the volume of particle j, which is defined as the mass M_j divided by the density of the particle ρ_j.

The Kernel $w(x\text{-}x_j)$ is a smoothing function and varies with the distance from x. When the Kernel smoothing length l and interparticle spacing Δx are small, the Kernel is assumed to have compact support, and thus the sum is only taken from neighboring particles.

The SPH method usually considers the fluid as compressible, and directly calculates the pressure from an equation of the state. The conservation of mass and the conservation of the momentum are written in particle form:

$$\frac{d\rho_i}{dt} = -\sum_j m_j (u_i - u_j) \cdot \nabla w(x_i - x_j) \tag{4}$$

$$\frac{d\mathbf{u}_i}{dt} = -\sum_j^N m_j \left(\frac{P_j}{\rho_j^2} + \frac{P_i}{\rho_i^2}\right) \nabla w(x_i - x_j) + \sum_j^N f_j w(x_i - x_j) / \rho_j \tag{5}$$

where u_i is velocity of particle, ρ_i is density of the particle, P_j is pressure at the particle, m_j is mass of the particle j, f_j is the external force including the gravity and the boundary friction force, and Π_{ij} is an empirical term representing the effects of viscosity [7]:

$$\Pi_{ij} = \begin{cases} -\alpha \mu_{ij} + \beta \tilde{c}_{ij} \mu_{ij}^2 & (\mathbf{u}_i - \mathbf{u}_j)(x_i - x_j) < 0 \\ 0 & elsewhere \end{cases} \tag{6}$$

Where and are emiprical coefficients, $\tilde{c}_{ij} = (c_i + c_j)/2$ and $\mu_{ij} = \ell(\boldsymbol{u}_i - \boldsymbol{u}_j)(x_i - x_j)/(\gamma_{ij}^2 + 0.01h^2)$.

The parameters and are often taken as 0.01-0.1. Thus, the stabilized discrete momentum equations becomes:

$$\frac{d\mathbf{u}_i}{dt} = -\sum_j m_j \left(\frac{P_j}{\rho_j^2} + \frac{P_i}{\rho_i^2} + \Pi_{ij}\right)\nabla w(x_i - x_j) \tag{7}$$

The fluid was treated as slightly compressible in this method [7]. The relationship between pressure and density was assumed as [20]:

$$p = B\left[\left(\frac{\rho}{\rho_0}\right)^{\gamma} - 1\right] \tag{8}$$

where $\gamma = 7$ and $B = 100 \quad {}_0H/\gamma$, with water density $\quad {}_0 = 1000$ kg/m^3, and water depth H.

2.2. Sph Method for Erosion Process

Shear stress for the erosion process can be obtained as [18]:

$$\tau = k\theta^n \tag{9}$$

where τ is the shear stress, k is the shear stress constant, taken as 1.0. θ is the shear rate and n is the flow behaviour index, taken as 0.5.

The shear rate can be approximated as:

$$\theta = v_{rel} / l_{rel} \tag{10}$$

where l_{rel} is the distance between flow particle and landform particle. v_{rel} is the relative velocity between flow particle and landform particle.

The erosion rate is formulated as:

$$\varepsilon = k_\varepsilon(\tau - \tau_c) \tag{11}$$

where k_ε is the erosion strength and τ_c is the critical shear stress. When l_{rel} is less than smoothing length and τ is greater than τ_c, erosion happens.

For HPTRM-strenghened levee, Pan et al. [6] and Li et al. [21] conducted full-scale overtopping tests and developed empirical relationship between erosion rate and shear stress and overtopping velocity. The empirical parameters for crticial shear stress is 10 Pa, and erosion strength is $1.2\text{x}10^{-8}$, which are only valid for this type of HPTRM material and grass system [21].

The SPH discrete form of mass change is expressed as:

$$dM_i / dt = -\sum_j l^2 \varepsilon(j) \tag{12}$$

where M_i is the mass of landform particle.

2.3. Conceptual Model

The conceptual model of a levee embankment strengthened by HPTRM along the crest and landward-side slope is shown in Fig. 2a. The width of the levee crest along the flow direction is 2 m. The seaward side has a slope of 1*V*:4.25*H*, and the landward-side slope has slope of 1*V*:3*H*.

2.4. Boundary Treatment

In this study, two types of boundary treatments, namely, ghost particles and solid particles were used. Ghost particles (type I) were assigned along the entire boundary (Fig. 3a). Negative water depth and velocity of real particles were used for the ghost particles to keep the pressure and velocity of the boundary equal to zero. Solid boundary particles (type II) were assigned along the ground surface and the levee profile (Fig. 3b). Since the HPTRM system is located on the crest and landward side slope of the levee, the solid boundary particles on this part required special treatment. Each particle in this area has its own mass, position and volume, where they can be eroded by the flow. The mass change is used to represent the erosion in every time step and the decreased value is the eroded mass (Fig. 3c). Once they are fully eroded, this part would be removed from the simulation. Moreover, these solid particles provided a friction force to the flow. The bottom friction stress is determined by the HPTRM material and was calculated by the following equation [22]:

$$\tau_b = \rho C_D |U_b| U_b \tag{13}$$

where $_b$ is the bottom frictional stress, C_D is equivalent roughness, is the density of water, and U_b is the velocity in the grid point nearest the solid boundary. The equivalent roughness C_D is defined as:

$$C_D = (\frac{1}{K}\ln\frac{H - y''}{y''} + 8.5)^2 \tag{14}$$

where K is the von Karman constant, y'' is the average height of deflected grass, H is water thickness. Based on measurements in the full-scale overtopping laboratory tests [6], the average water thickness of H was taken as 0.1 m along the landward-side slope, y'' was taken as 0.0127 m, and K was taken as 0.4. The value of C_D of HPTRM system was then calculated as 0.019.

2.5. Erosion Treatment

When the boundary particles (type II) are in the smoothing circle of the flow particles, the flow particles would give shear stress to the boundary particles. If the shear stress is above the critical value, the erosion happens. As the erosion occurs, the first layer of wall particle is eroded, and then the solid boundary becomes uneven. The new wall and mirror particles are generated on the side to reflect The Eroded Boundary.

2.6. Intial Conditions

Initially, there were 9998 flow particles and 5332 solid boundary particles (type II) in the computational domain. The change in the number of ghost particles (type I) depends on the time. The surge overflow depth in the seaside was assumed to be constant during the computational time, after achieving steady-state surge overflow conditions. The wave is generated at 20 m far away from the seaward side slope toe. The initial input condition were three surge elevations (h_1 = +0.2, +0.4 and +0.6 m above the levee crest), three significant wave heights (H_{m0} = 0.3, 0.6 and 0.9 m), and three peak wave periods (T_p = 4, 5 and 6 s). This yielded a total of 27 unique conditions for combined wave and surge overtopping.

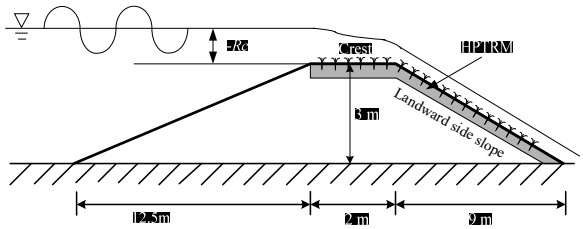

Fig. 2. Conceptual setup of earthen levee strengthened by HPTRM in the crest and landward-side slope under combined wave and surge overtopping. Freeboard R_c is defined as vertical distance between the still water elevation and crest elevation.

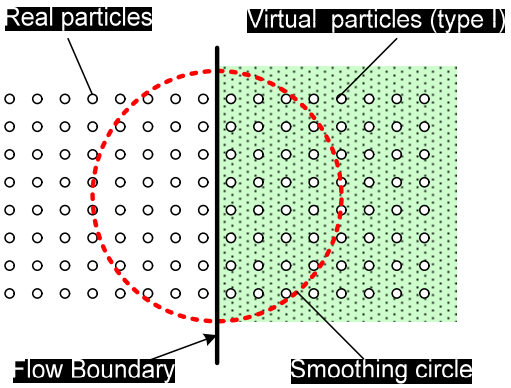

(a)

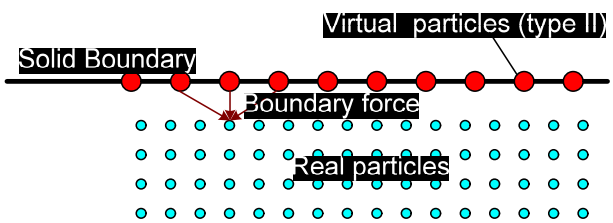

(b)

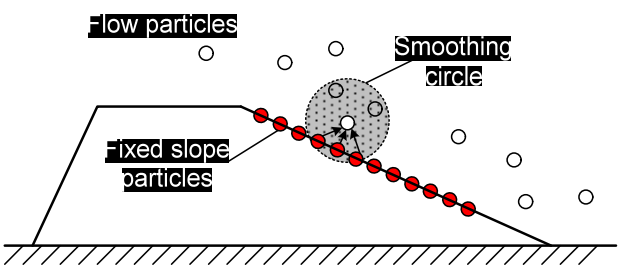

(c)

Fig. 3. Illustration of (a) ghost particles (type I), (b) solid boundary particles (type II), and (c) the erosion process.

Table 1: Hydrodynamic parameters and average wave overtopping discharge in the tests

Trail No.	h_1 (m)	H_{m0} (m)	T_p (s)	q_{ws} (m^3/s-m)	q_s (m^3/s-m)
1	0.2	0.285	3	0.21	0.16
2	0.2	0.305	4	0.18	0.16
3	0.2	0.310	5	0.19	0.16
4	0.2	0.622	3	0.21	0.16
5	0.2	0.593	4	0.22	0.16
6	0.2	0.597	5	0.21	0.16
7	0.2	0.902	3	0.23	0.16
8	0.2	0.912	4	0.25	0.16
9	0.2	0.880	5	0.29	0.16
10	0.4	0.285	3	0.46	0.40
11	0.4	0.305	4	0.43	0.40
12	0.4	0.310	5	0.41	0.40
13	0.4	0.622	3	0.46	0.40
14	0.4	0.593	4	0.41	0.40
15	0.4	0.597	5	0.47	0.40
16	0.4	0.902	3	0.43	0.40
17	0.4	0.912	4	0.55	0.40
18	0.4	0.880	5	0.42	0.40
19	0.6	0.285	3	0.77	0.80
20	0.6	0.305	4	0.75	0.80
21	0.6	0.310	5	0.79	0.80
22	0.6	0.622	3	0.82	0.80
23	0.6	0.593	4	0.85	0.80
24	0.6	0.597	5	0.87	0.80
25	0.6	0.902	3	0.82	0.80
26	0.6	0.912	4	0.92	0.80
27	0.6	0.880	5	0.77	0.80

Note: h_1 is difference between surge elevation and levee crest elevation ($h_1 = -R_c$), H_{m0} is energy-based significant wave height, and T_p is peak spectral wave period. q_s is surge-only steady overflow discharge per unit length, and q_{ws} is combined wave and surge overtopping discharge per unit length.

In this study, linked-list algorithm was used for the nearest neighboring particles searching algorithm, since it is more effective and easier to implement [23]. Kernel smoothing length l and interparticle spacing Δx was studied in a sensitivity analysis to assess how the SPH model is affected by these two key parameters. The sensitivity analysis found that interparticle spacing Δx should be 0.1 m or less, and the smoothing length l should be 2Δx or less in this study.

2.7. Numerical Wave Generator

Random waves were applied as the upstream (sea-side) boundary condition for water level. The random waves were generated using the parameterized Joint North Sea Wave Project (JONSWAP)-spectrum as [24]:

where $S(f)$ is the spectral density function, H_s is the significant wave height (= $H_{1/3}$; defined as average of highest 1/3 waves); T_p is the peak wave period, f is the wave frequency and ' is the spectral enhancement

factor, and is 0.07 for $T_p f \leq 1$ or 0.09 for $T_p f > 1$. The spectral enhancement parameter ' is in the range of 1 to 6 and has a normal distribution with a mean of 3.3 and a standard deviation of 0.79 [24].

3. Results and Discussion

Table 1 lists the input combined wave and surge parameters for all the 27 cases and the corresponding output discharge q_s and q_{ws}. The time series of flow thickness and time series of flow velocity at the same location were used to estimate the time series of overtopping discharge. The q_s is surge-only steady overflow discharge per unit length, and the q_{ws} is combined wave and surge overtopping discharge per unit length. The q_s is the average of the first 50 discharge data points taken as the steady overflow discharge at the middle of levee crest, and q_{ws} is the average for 500 instantaneous discharge data points at the middle of levee crest. These 500 data points did not include any data from the initial steady overflow portion prior to waves arriving at the levee. In addition to the overtopping discharge output, flow thickness and horizontal velocity are also output for each simulation case. Fig. 4 provides an example of the SPH simulated instantaneous flow thickness, horizontal velocity and discharge for a 16-36 s time series at the middle of levee crest.

$$S(f) = \frac{0.06238\left(1.094 - 0.01915\ln\gamma'\right)}{0.230 + 0.0336\gamma' - 0.185\left(1.9 + \gamma'\right)^{-1}} H_s^2 T_p^{-4} f^{-5} \exp\left(-1.25 T_p^{-4} f^{-4}\right) \gamma'^{\exp\left(-\left(T_p f - 1\right)^2 / 2\sigma^2\right)} \qquad (15)$$

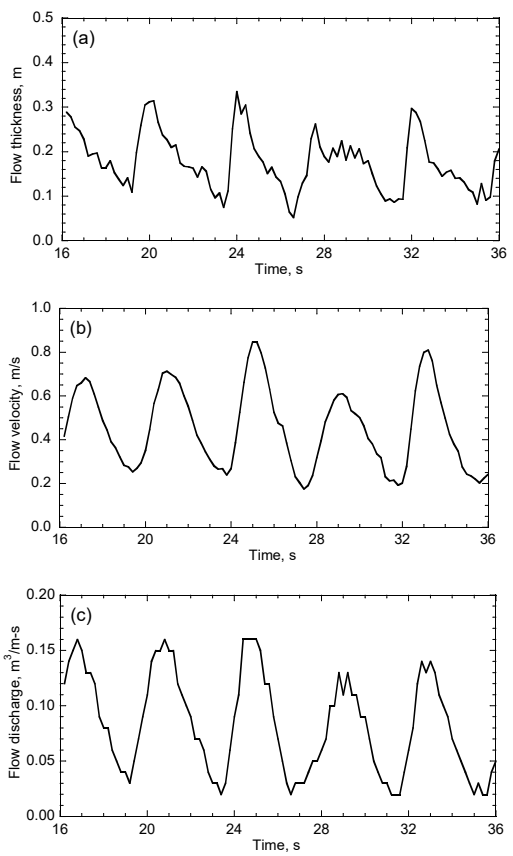

Fig. 4. Example of SPH simulated flow thickness (a), horizontal flow velocity (b), and overtopping discharge (c) at middle of levee crest

3.1. Average Overtopping Discharge for Combined Wave and Surge Overtopping

The wave overtopping discharge rate is a critical parameter in the conceptual and preliminary design of levees. Based on physical experiments and numerical models, several empirical formulae have been developed to predict overtopping of levees under given wave conditions and water levels [1, 25, 26]. The overtopping discharge depends on wave parameters and structure parameters, including the seawall freeboard, the crest geometry, the seaward slope, the significant wave height, the mean or peak wave period, the angle of wave attack measured from the normal to the structure, the water depth at the toe of the seawall, and the seabed slope. Hughes and Nadal [1] provided a detailed review for the overtopping discharge for surge overflow, wave overtopping, and combined wave and surge overtopping conditions.

Fig. 5 presents the dimensionless combined wave/surge average overtopping discharge as a function of the relative freeboard for all 27 cases. The predication made by the calibrated SPH model also compares well with the full-scale overtopping test results. The best fit curve to the SPH predications yields a nice trend with increasing relative freeboard. The solid line is a best-fit empirical equation given by the formula

$$q_{ws} / \sqrt{gH_{m0}^3} = 0.01 + 0.57(-R_C / H_{m0})^{1.27}, \quad R_c < 0 \qquad (16)$$

where q_{ws} is the combined wave and surge overtopping discharge per unit length, H_{m0} is the energy-based significant wave height, g is the gravitational acceleration constant, and freeboard R_c is defined as the vertical distance between the still water elevation and crest elevation.

Note that R_c must be entered as a negative number so the ratio in brackets will be positive. Peak spectral wave period had a negligible influence on the determination of q_{ws} for the range of periods tested in the model. This finding is consistent with Hughes and Nadal [1] and Pan et al. [6]. It may be noted that the application of Equation 16 is limited to the levee geometry with a seaward-side slope of $1V$:4.25H, and the roughness of the protective system being similar to HPTRM.

Fig. 5 also plots the estimates from the empirical equations of Hughes and Nadal [1], Schüttrumpf et al. [25], Reeve et al. [26] and full scale lab data [6]. All the prediction methods for naked levee overestimated the measurements with the equations of Hughes and Nadal [1] showing the greatest agreement. As shown in Fig. 5, the SPH prediction is higher than full scale laboratory measurements when R_c/H_{m0} < -0.2, but is lower than numerical prediction by Reeve et al. [26]. The SPH model estimated discharge by counting number of particles flowing through a certain location per second. The discharge equals the number multiply by the volume of each particle. Since some particles may not fully pass through the location, the full particle volume was used to calculate the discharge, and thus the discharge may be overestimated. The predications made by Schüttrumpf's and Reeve et al. [25, 26] are too far from the measured data, which was also observed also by the Hughes and Nadal [1].

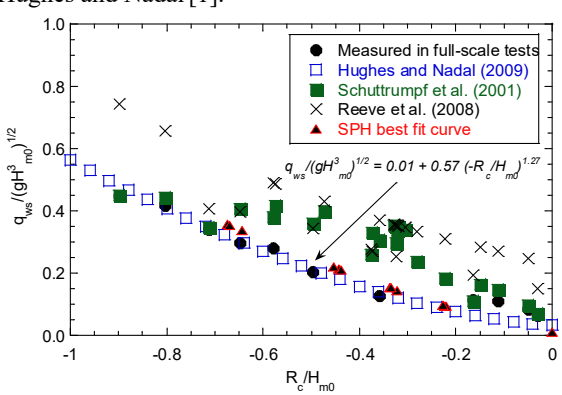

Fig. 5. SPH simulated dimensionless combined wave/surge average discharge and estimation of overtopping discharge using full-scale overtopping tests and equations of Schüttrumpf et al. (2001), Reeve et al. (2008) and Hughes and Nadal (2009).

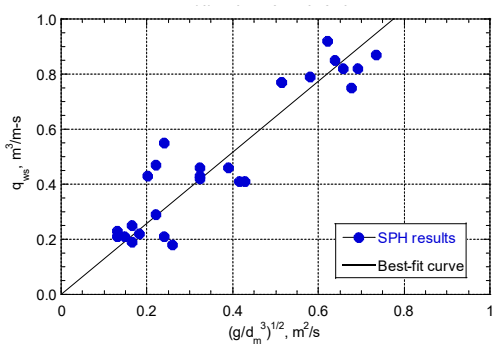

Fig. 6. The relationship between the combined wave average overtopping discharge and mean flow thickness on the landward slope for SPH modeling results

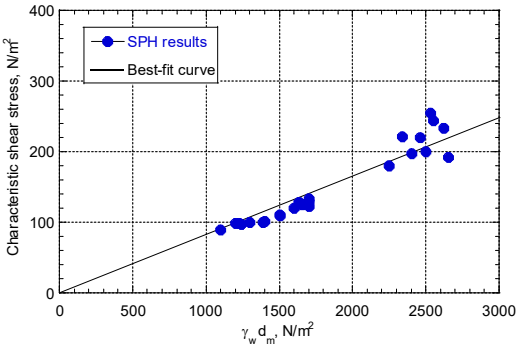

Fig. 7. Estimation of the root-mean-square of the shear stress by the product of the unit weight of fresh water and the mean flow thickness.

3.2. Analysis of soil loss

3.2.1. Estimation of shear stresses on landward-side slope

Based on full-scale overtopping test in Pan et al. [6], the flow down the landward-side slope caused by combined waves and surge overtopping case can reach a balance after which the characteristic values of the flow (e.g. average flow thickness and flow velocity, RMS flow thickness and velocity) remain unchanged along the landward-side slope. On the landward-side slope, the statistical hydraulic parameters remain essentially unchanged from middle of landside slope to the toe. Thus, the shear stress calculated at middle of landside slope can represent the shear stress condition on landward-side slope.

Fig. 6 shows the relationship between the combined wave average overtopping discharge and mean flow thickness on the landward slope for all 27 cases. The best fit curve to the SPH predications yields a nice linear trend, and the best-fit empirical equation is given by the formula:

$$q_{ws} \Big/ \sqrt{g d_m^3} = 1.3 \tag{17}$$

where q_{ws} is the combined wave and surge overtopping discharge per unit length, g is the gravitational acceleration constant, d_m is the mean flow thickness on landward-side slope. Pan et al. [6] obtained similar equation with coefficient of 2.362 based on their full-scale overtopping tests. The difference is caused by the overestimation of SPH free surface prediction.

Time series of shear stress at the middle of landside slope were calculated. An empirical relationship was developed between the hydrodynamic parameters for each experiment and the corresponding root-mean-square of the shear stress. As shown in Fig. 7, linear relationship was found between the root-mean-square of the average shear stress and the unit weight of fresh water, γ_w, and the average flow thickness on landward-side slope, d_m, as:

$$\tau_{t,rms} = 0.083 \gamma_w d_m \tag{18}$$

Pan et al. [6] obtained a similar equation with coefficient of 0.0547 from their full-scale overtopping tests. The SPH result has the same trend but provides higher value for $\tau_{t,rms}$ than the full scale tests.

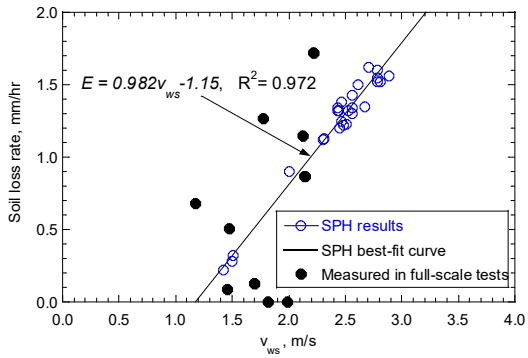

Fig. 8. Comparison of SPH simulated erosion rate and measured in full-scale tests at *S4*. *S4* is located along the landward-side slope of the levee embankment during the combined wave and surge overtopping conditions.

3.2.2. Soil loss

During this study, after each test, soil loss rate was calculated at the middle of landside slope. Average overtopping flow velocity at the middle of landside slope was examined to find a relationship between soil loss rate and hydraulic condition. The best fit relationship between soil loss rate and the average overtopping flow velocity for the 27 cases at the middle of landside slope is shown in Fig. 8.

As shown in Fig. 8, erosion starts when the average overtopping flow velocity exceeds 1.4 m/s. The average overtopping flow velocity of 1.4 m/s is a threshold of soil loss from HPTRM. Beyond this threshold, the relation between erosion rate and average overtopping flow velocity is approximately linear.

4. Conclusions

A SPH numerical method was developed in this study to analyze and predict the overtopping hydraulics of a levee strengthened by HPTRM subjected to combined wave and surge overtopping. A combination of 27 hydraulic cases was studied. The overtopping discharge, flow thickness, flow velocity, average overtopping velocity, shear stress, and soil erosion rate wee calculated. The main conclusions and findings of the present numerical investigation are summarized below:

- An equation was developed that expresses the average overtopping discharge per unit length along the levee crest as a function of negative freeboard and incident energy-based significant wave height. The new equation fits the data quite well, and gives lower overtopping rates than previous numerical equations. The equation can be used by practical engineer to design the levee systems.
- Average flow thickness was found to influence the RMS shear stress on levee landward-side slope. An empirical equation was developed to estimate the root-mean-square of the shear stress on the landward-side slope. Soil erosion rate at the landward-side slope was found to be related to the average overtopping flow velocity.
- All the equations developed in this paper are based on the HPTRM on a levee embankment session with a seaside slope of 1*V*:4.25*H* and a landward-side slope of 1*V*:3*H*. The equations associated with unsteady flow on the landward-side slope may not be applicable for levees with different slopes.

Acknowledgment

This research was funded by the Department of Homeland Security-sponsored Southeast Region Research Initiative (SERRI) at the Department of Energy's Oak Ridge National Laboratory. The opinions and conclusions described in this paper are solely those of the authors and do not necessarily reflect the opinions or policies of the sponsors.

References

A. Colagrossi and M. Landrini, Numerical Simulation of Interfacial Flows by Smoothed Particle Hydrodynamics. Journal of Computational Physics 191 (2003) 448-475.

A. Shakibaeinia, and Y. Jin, A Mesh-Free Particle Model for Simulation of Mobile-Bed Dam Break. Advances in Water Resources 34 (2011) 794-807.

ASCE Hurricane Katrina External Review Panel, The New Orleans Hurricane Protection System: What Went Wrong and Why? American Society of Civil Engineers, Reston, Virginia. (2007) 92 pp.

D. E. Reeve, A. Soliman,and P. Z. Lin, Numerical Study of Combined Overflow and Wave Overtopping over a Smooth Impermeable Seawall. Coastal Engineering 55 (2008) 155-166.

G. K. Batchelor, An Introduction to Fluid Mechanics. Cambridge University Press (1974).

G. L. Sills, N. D. Vroman, R. E. Wahl, and N. T. Schwanz, Overview of New Orleans levee failures: Lessons learned and their impact on national levee design and assessment. Journal of Geotechnical and Geoenvironmental Engineering, 134 (2008) 556-565.

G. Oger, M. Doring, B. Alessandrini, P. Ferrant, An Improved SPH Method: Towards Higher Order Convergence. Journal of Computational Physics 225 (2007) 1472-1492.

Goda, A Comparative Review on the Functional Forms of Directional Wave Spectrum. Coastal Engineering Journal, 41 (1999) 1-20.

H. Schüttrumpf, J. Möller, H. Oumeraci, J. Grüne, and R. Weissmann, Effects of Natural Sea States on Wave Overtopping of Seadikes. Proceedings of the 4th International Symposium Waves 2001, Ocean Wave Measurement and Analysis 2 (2001) 1565–1574.

J. Fang, A. Parriaux, M. Rentschler, and C. Ancey, A Improved SPH Methods for Simulating Free Surface Flows of Viscous Fluids. Applied Numerical Mathematics 59 (2009) 251-271.

J. J. Monaghan, Smoothed Particle Hydrodynamics. Reports on Progress in Physics 68 (2005) 1703-1759.

J. L. Briaud, H. C. Chen, A. V. Govindasamy, and R. Storesund, Levee Erosion by Overtopping in New Orleans during the Katrina Hurricane. Journal of Geotechnical and Geoenvironmental Engineering, 134 (2008) 618-632.

J. Ubilla, T. Abdoun, I. Sasanakul, M. Sharp, S. Steedman, W. Vanadit-Ellis, and T. Zimmie, New Orleans Levee System Performance during Hurricane Katrina: London Avenue and Orleans Canal South. Journal of Geotechnical and Geoenvironmental Engineering, 134 (2008) 668-680.

J.J. Monaghan, Simulating Free Surface Flows with SPH. Journal of Computational Physics, 110 (1994) 399-406.

L. Li, F. Amini, Y. Pan, C. P. Kuang, and J. Briaud, Erosion Resistance of HPTRM Strengthened Levee from Combined Wave and Surge Overtopping, Journal of Geotechnical and Geological Engineering, DOI 10.1007/s10706-014-9762-7 (2014).

M. B. Liu, G. R. Liu, and K. Y. Lam, Investigations into Water Mitigations using a Meshless Particle Method, Shock Waves, 12 (2002) 181-195.

M. Gomez-Gesteira, D. Cerqueiro, C. Crespo, R. A. Dalrymple, Green Water Overtopping Analyzed with a SPH Model. Ocean Engineering 32 (2005) 223–238.

P. Liu, P.Z. Lin, K.A. Chang, and T. Sakakiyama, Numerical Modeling of Wave Interaction with Porous Structures. Journal of Waterway, Port, Coastal, and Ocean Engineering, 125 (1999) 322–330.

R. A. Dalrymple, and B.D. Rogers, Numerical Modeling of Water Waves with the SPH method. Coastal Engineering, 53 (2006) 141-147.

R. Ata, and A. Soulaimani, A Stabilized SPH Method for Inviscid Shallow Water Flows. International Journal for Numerical Methods in Fluids, 47 (2005) 139-159.

S. Shao, C. Ji, D. I. Graham, D. E. Reeve, P. W. James, and A. J. Chadwick, Simulation of Wave Overtopping by an Incompressible SPH Model. Coastal Engineering, 53 (2006) 723-735.

S.A. Hughes and N.C. Nadal, Laboratory Study of Combined Wave Overtopping and Storm Surge Overflow of a Levee. Coastal Engineering, 56 (2009) 244–259.

T. Li, P. Troch, and J. De Rouck, Wave Overtopping over a Sea Dike. Journal of Computational Physics, 198 (2004) 686–726.

U. Stephan, and D. Gutknecht, Hydraulic Resistance of Submerged Flexible Vegetation. Journal of Hydrology, 269 (2002) 27-43.

X. Rao, L. Li, F. Amini, and H. Tang, SPH Modeling of Combined Wave and Surge Overtopping and Hydraulic Erosion of ACB Strengthened Levee System.. Journal of Coastal Research 28 (2012) 1500-1511.

Y. Pan, L. Li, F. Amini, and C. P. Kuang, Full Scale HPTRM Strengthened Levee Testing under Combined Wave and Surge Overtopping Conditions: Overtopping Hydraulics, Shear Stress and Erosion Analysis. Journal of Coastal Research 29 (2013) 182-200.